© 2023. Published by The Company of Biologists Ltd | Journal of Cell Science (2023) 136, jcs260740. doi:10.1242/jcs.260740

RESEARCH ARTICLE

Lfc subcellular localization and activity is controlled by αv-class integrin

Georgina P. Coló*,‡, Andrea Seiwert and Raquel B. Haga

ABSTRACT

Fibronectin (FN)-binding integrins control a variety of cellular responses through Rho GTPases. The FN-binding integrins, αvβ3 and α5β1, are known to induce different effects on cell morphology and motility. Here, we report that FN-bound αvβ3 integrin, but not FN-bound α5β1 integrin, triggers the dissociation of the RhoA GEF Lfc (also known as GEF-H1 and ARHGEF2 in humans) from microtubules (MTs), leading to the activation of RhoA, formation of stress fibres and maturation of focal adhesions (FAs). Conversely, loss of Lfc expression decreases RhoA activity, stress fibre formation and FA size, suggesting that Lfc is the major GEF downstream of FN-bound αvβ3 that controls RhoA activity. Mechanistically, FN-engaged αvβ3 integrin activates a kinase cascade involving MARK2 and MARK3, which in turn leads to phosphorylation of several phospho-sites on Lfc. In particular, S151 was identified as the main site involved in the regulation of Lfc localization and activity. Our findings indicate that activation of Lfc and RhoA is orchestrated in FN-adherent cells in an integrin-specific manner.

KEY WORDS: Integrin, Fibronectin, Signalling, Lfc, GEF-H1, Rho GTPase, Actin dynamics, MARK2, MARK3

INTRODUCTION

Integrins connect cells to a wide range of extracellular matrix (ECM) proteins, including fibronectin (FN), vitronectin (VN), collagens and laminins, as well as to other cell surface receptors such as VCAMs and ICAMs. Mammals express 18 α-integrin and eight β-integrin subunits, which assemble into 24 functionally distinct integrin receptors, binding to different ECM proteins and resulting in the transduction of several intracellular signals (Hynes, 2002). Most cell types simultaneously express a number of integrin subtypes, which can synergize to amplify signals and transmit information via a large signalling hub called the adhesome (Hynes, 2002; Schiller and Fässler, 2013; Schiller et al., 2013; Roca-Cusachs et al., 2009; Kuo et al., 2011). Integrin specificity plays a major role in signalling from ECM proteins into cells. The individual role of integrin receptors that bind to the same ECM ligand is still not completely understood.

Genetically manipulated cells are valuable tools to elucidate integrin-specific functions (Danen et al., 2002). For example, pan-integrin knockout (pKO) murine fibroblasts (Schiller et al., 2013) expressing either αvβ3 (pKO-αv fibroblasts) and/or α5β1 integrin (pKO-β1 and pKO-αv,β1 fibroblasts), and Chinese hamster ovary (CHO) cells overexpressing either β1 or β3 integrin (Miao et al., 2002) have been used to reveal that an increase of RhoA activity and formation of stress fibres and focal adhesions (FAs) is more pronounced upon αvβ3 integrin than α5β1 integrin binding to FN. Nonetheless, the role of β1 integrins in RhoA activation should not be neglected, as other cell systems have shown more pronounced RhoA signalling in the presence of β1 integrins compared with αvβ3 integrins (Costa et al., 2013; Danen et al., 2002; Vial et al., 2003). RhoA is a classic member of the Rho GTPase family that cycles between an active GTP-bound and an inactive GDP-bound form, as controlled by guanine nucleotide exchange factors (GEFs) and GTPase-activating proteins (GAPs), respectively (Haga and Ridley, 2016; Marjoram et al., 2014). However, how αvβ3 integrin activates RhoA in a more pronounced way than α5β1 in fibroblasts and CHO cells is not clear.

One of the major GEFs that activates RhoA is Lfc (also known as GEF-H1 and ARHGEF2 in humans). Lfc activity is tightly controlled, with inactive Lfc sequestered on polymerized microtubules (MTs) (Ren et al., 1998; Birkenfeld et al., 2008), whereas activation of Lfc requires its release from MTs (Krendel et al., 2002). The MT release can be mediated by phosphorylation of Lfc on specific threonine and/or serine residues, MT depolymerization or dissociation of Lfc from the MT-associated Tctex-1 (DYNLT1)–dynein intermediate chain (DIC) complex in response to lysophosphatidic acid (LPA) or thrombin stimulation, mediated by the G-protein Gα13 (GNA13) (Krendel et al., 2002; Meiri et al., 2014; Chang et al., 2008). Once Lfc is released and activated, it promotes the GDP to GTP exchange of RhoA, which results in RhoA activation, the recruitment of RhoA effector proteins such as mDia1 (DIAPH1), and actin polymerization (Narumiya et al., 2009).

Here, we investigated how Lfc is activated by αvβ3 integrin. We show that FN-mediated αvβ3 integrin engagement induces Lfc-activation via phosphorylation, which results in Lfc translocation from MTs to the cytoplasm, inducing stress fibre and FA formation.

RESULTS

GEF activation in pKO cells

It has previously been shown that FN-seeded pKO mouse fibroblasts expressing FN-binding αv-class integrins (pKO-αv fibroblasts) display higher RhoA activity, thicker stress fibres and larger FAs than pKO mouse fibroblasts expressing α5β1 integrin (pKO-β1 fibroblasts) or pKO mouse fibroblasts expressing both αvβ3 and α5β1 integrins (pKO-αv,β1) (Schiller et al., 2013). The three cell lines have different actin filament distribution (Fig. 1A; Fig. S1A). Quantification showed that pKO-β1 cells had less fluorescence intensity of actin staining than pKO-αv and pKO-αv,

Department of Molecular Medicine, Max Planck Institute of Biochemistry, Am Klopferspitz 18, 82152, Martinsried, Germany.
*Present address: Instituto de Investigaciones Bioquímicas de Bahía Blanca (CONICET), Departamento de Biología, Bioquímica y Farmacia, Universidad Nacional del Sur, 8000 Bahía Blanca, Argentina

‡Author for correspondence (gcolo@inibibb-conicet.gob.ar)

G.P.C., 0000-0003-3476-8387; R.B.H., 0000-0001-5930-3311

Handling Editor: Arnoud Sonnenberg
Received 21 October 2022; Accepted 31 March 2023

Journal of Cell Science (2023) 136, jcs260740. doi:10.1242/jcs.260740

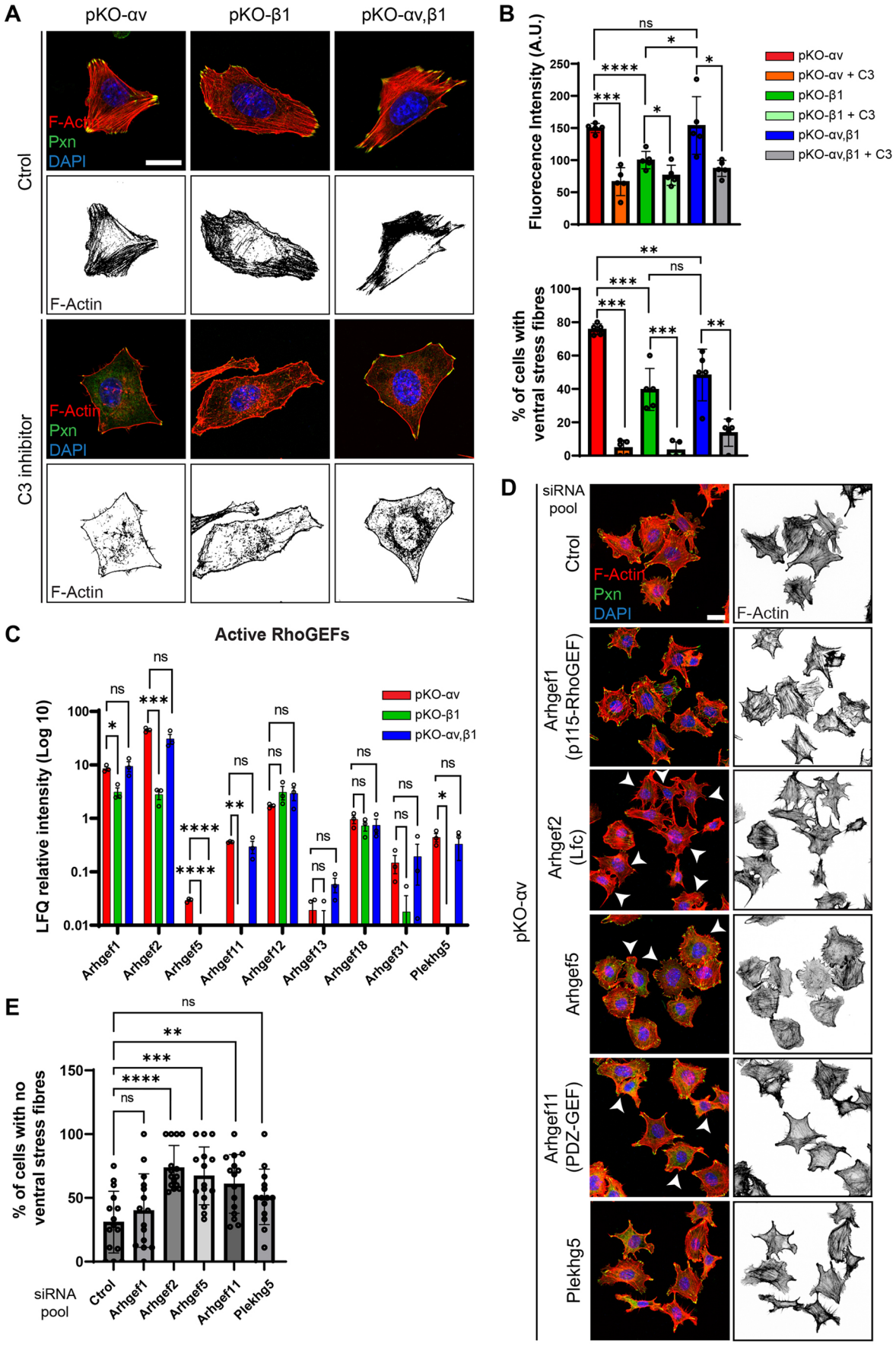

Fig. 1. See next page for legend.

Journal of Cell Science

Journal of Cell Science (2023) 136, jcs260740. doi:10.1242/jcs.260740

Fig. 1. Differential GEF activation in pKO cells. (A) Immunostaining of indicated cell types plated on FN for 4 h in serum-free medium with either vehicle control or the C3 transferase rho inhibitor. The merged images show an overlay of F-actin (red), paxillin (green) and nuclei (DAPI, blue). Images are representative of two independent experiments. Scale bar: 10 µm. (B) Quantification of F-actin fluorescence intensity and the percentage of cells with ventral stress fibres. Graphs show quantification of three independent experiments. **P*<0.05; ***P*<0.01; ****P*<0.001; *****P*<0.0001; ns, not significant (unpaired two-tailed *t*-test between pKO-αv, pKO-β1 and pKO-αv,β1 and pKO cells and the respective pKO cells+C3 inhibitor). A.U., arbitrary units. Results are mean±s.d. (C) Bar graph showing MS intensity of nine GEFs in the indicated cell types from three independent experiments. There were significant MS intensity changes among the cell types **P*<0.05; ***P*<0.01; ****P*<0.001; *****P*<0.0001; ns, not significant (one-way ANOVA followed by Dunnett's test). Results are mean±s.e.m. (D) Immunostaining of pKO-αv cells after transfection with indicated GEF-targeting siRNA pool. The merged images show an overlay of paxillin (green), F-actin (red) and nuclei (DAPI, blue). White arrowheads indicate cells that lost ventral stress fibres. Images are representative of three independent experiments. Scale bar: 20 µm. (E) Quantification of cells with no ventral stress fibres in relation to total cells after siRNA transfection targeting indicated GEFs. Graph shows the quantification of 50–100 cells per condition from three independent experiments. ***P*<0.01, ****P*<0.001 and *****P*<0.0001 (ordinary one-way ANOVA followed by Dunnett's test between control and siRNA pools). Results are mean±s.d.

β1 cells (Fig. 1B) and that pKO-β1 and pKO-αv,β1 cells exhibited fewer ventral stress fibres compared to that seen in pKO-αv cells (Fig. 1B). To confirm the importance of Rho activity in the formation of FA and stress fibre assembly in the pKO cell lines, we treated FN-seeded pKO-αv, pKO-β1 and pKO-αv,β1 fibroblasts with C3 transferase, a well-known Rho inhibitor (Barbieri et al., 2002), which inhibits RhoA and its close relatives RhoB and RhoC. All three cell lines had reduced stress fibres and FAs following C3 transferase treatment (Fig. 1A,B), indicating that activated Rho promotes stress fibre formation downstream of FN-engaged αv- as well as β1-class integrins.

RhoA activity is controlled by many different GEFs and GAPs (Hodge and Ridley, 2016). To identify the GEFs that are activated by specific FN-binding integrin receptors, we performed pulldown assays with cell lysates from all three pKO cell lines using recombinantly expressed and purified GST-tagged RhoA G17A (a nucleotide-free mutant), which binds active GEFs (García-Mata et al., 2006; Guilluy et al., 2011). Interacting GEFs were identified using mass spectrometry (MS; Fig. S1B). We identified nine different Rho GEFs that interacted with GST–RhoA G17A. Five out of the nine RhoA GEFs showed significantly higher activity in αv-class integrin-expressing fibroblasts (Fig. 1C), and Lfc/Arhgef2 was the GEF that bound to RhoA G17A with the highest abundance. Total proteome analysis revealed equal expression levels of the different GEFs in all three cell lines (Fig. S1C). Although we could detect low levels of active Arhgef5, enriched via the pulldown assay, the total protein in our MS assays was not detectable in any of the cell lines. To identify which of the five GEFs are responsible for the pronounced stress fibre levels in pKO-αv fibroblasts, we transiently and individually depleted the GEFs and investigated their impact on ventral stress fibre formation (Fig. 1D). The experiments revealed that out of the five RhoA GEFs tested, depletion of Lfc/Arhgef2, Arhgef5 and Arhgef11 decreased ventral F-actin stress fibres (Fig. 1D,E), with Lfc depletion showing the most consistent and highest effect compared to that seen on Arhgef5 and Arhgef11 depletion (Fig. 1E). Based on these results, we decided to investigate the role of Lfc in RhoA activation, stress fibre formation and FA maturation in pKO cells.

αv-class integrins induce Lfc- and RhoA-mediated stress fibre formation

To determine how Lfc affects integrin class-specific stress fibre and FA formation, we deleted the Lfc-encoding *Arhgef2* genes (Lfc KO) in pKO-αv, pKO-β1 and pKO-αv,β1 fibroblasts using the Crispr/Cas9 gene editing technology and confirmed the successful KOs via western blotting (Fig. S2A). The different cell lines were seeded on FN-coated circular micropatterns to analyse F-actin organization (Fig. 2A). Loss of Lfc expression in pKO-αv and pKO-αv,β1 fibroblasts reduced the number of organized stress fibres and the length of ventral stress fibres, increased the amount of circular actin filaments in the cell periphery, with an increase in number of junctions, and resulted in a decrease in the number of large FAs (>3 µm) (Fig. 2A,B; Fig. S2B). Loss of Lfc in pKO-β1 fibroblasts also led to reduced number of organized stress fibres and length of ventral stress fibres, with loss of central adhesions and a decrease in number of small adhesions (<3 µm) (Fig. 2A,B; Fig. S2B). Re-expression of Lfc in the pKO cells rescued the phenotype of stress fibre formation in all three cell lines (Fig. S2C).

Next, we tested how loss of Lfc expression affects RhoA activity in the pKO cell system. In line with the previous report of Schiller et al. (2013), the levels of RhoA activity were higher in pKO-αv fibroblasts than in pKO-β1 and pKO-αv,β1 fibroblasts cultured for 45 min on FN (Fig. 2C). Deletion of *Arhgef2* genes decreased RhoA activity in pKO-αv fibroblasts compared to that in pKO-αv WT cells. Given that RhoA activity remained unaffected by *Arhgef2* loss in pKO-β1 fibroblasts (Fig. 2C), we conclude that Lfc plays an important role on RhoA activation downstream of FN-engaged αvβ3 integrins. Western blots of Lfc after pulldown with GST-tagged RhoA G17A demonstrated that pKO-αv fibroblasts contained more active Lfc than pKO-β1 and pKO-αv,β1 fibroblasts (Fig. 2D), confirming that αv-class integrin engagement increases Lfc activity, which in turn leads to RhoA activation and the formation of thick, ventral F-actin fibres connected to large FAs.

αvβ3 integrin engagement induces the release of Lfc from MTs

Inactive Lfc is sequestered on MTs, whereas active Lfc is released into the cytoplasm (Krendel et al., 2002). Immunostaining revealed that Lfc was predominantly localized in the cytoplasm of FN-seeded pKO-αv fibroblasts, whereas the majority of Lfc colocalized with the MTs in pKO-β1 fibroblasts (Fig. 3A,B). pKO-αv,β1 fibroblasts exhibited an intermediate Lfc distribution between the MTs and cytosol (Fig. 3A,B). Note that no clear difference in MT distribution was observed between the three cell lines (Fig. 3A).

To confirm that FN engagement of αv-class integrins suffices to release Lfc from MTs, we seeded wild-type (WT) mouse fibroblasts on glass coverslips coated with either an α5β1- or cRGD-αvβ3-specific peptidomimetic (Rechenmacher et al., 2013) and determined Lfc localization. WT fibroblasts cultured on αvβ3 peptidomimetic had substantial amounts of Lfc in the cytoplasm and adopted a polygonal shape with few lamellipodium-like membrane protrusions (Fig. 3C,D), whereas the WT fibroblasts seeded on α5β1 peptidomimetic predominantly showed Lfc colocalized with MTs and developed multiple membrane protrusions (Fig. 3C,D). The actin cytoskeleton phenotype is similar to that of pKO-αv cells and pKO-β1, respectively, when cultured on fibronectin (Fig. S1A; Schiller et al., 2013). To corroborate the findings, we seeded EGFP-tagged Lfc-expressing WT fibroblasts on either FN- or VN-coated glass coverslips and blocked αv-class or α5β1-class integrins with cilengitide or β1 integrin-blocking antibody (Hermann et al., 2016), respectively.

Journal of Cell Science (2023) 136, jcs260740. doi:10.1242/jcs.260740

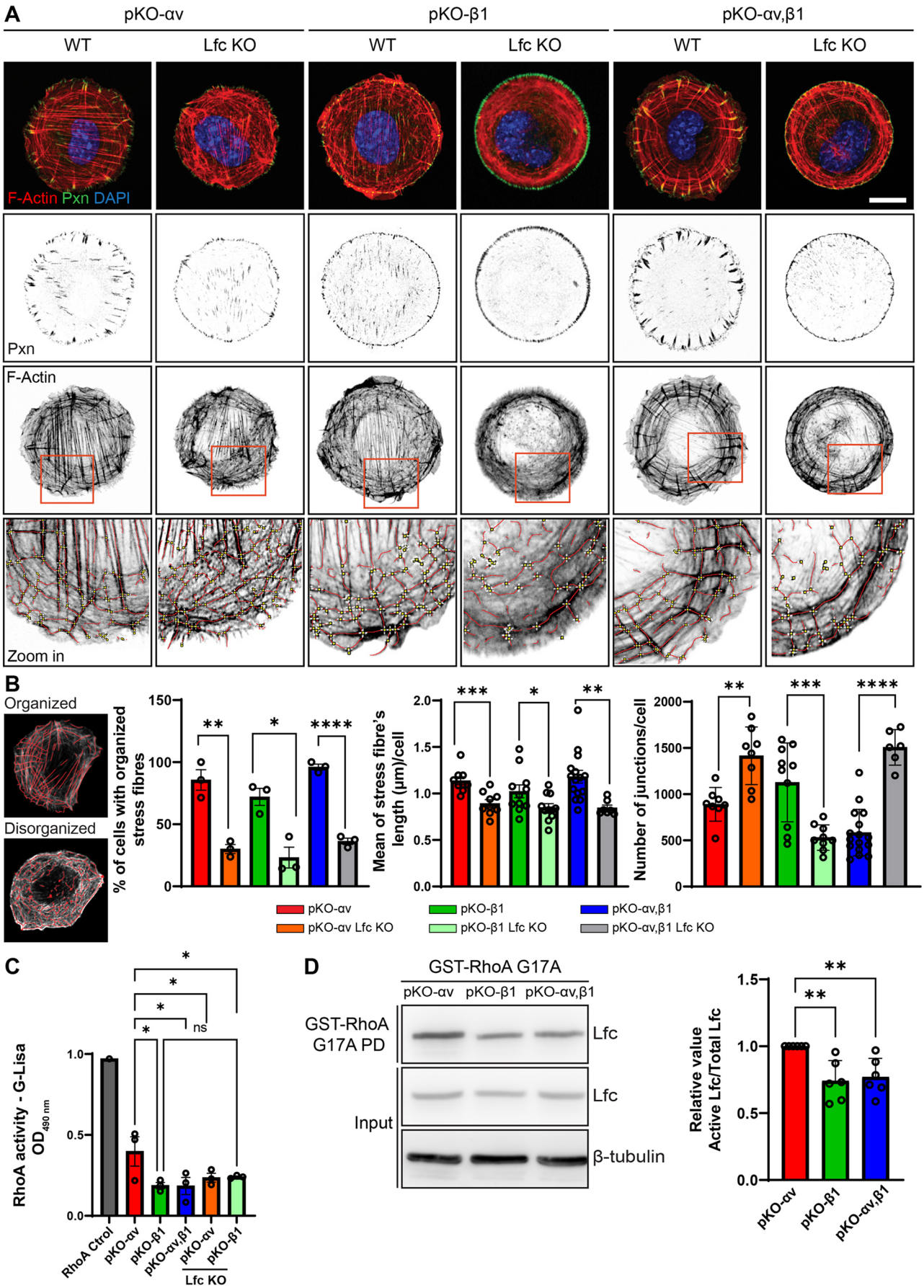

Fig. 2. See next page for legend.

Journal of Cell Science (2023) 136, jcs260740. doi:10.1242/jcs.260740

Fig. 2. αv-class integrins induce Lfc and RhoA activation and stress fibre formation. (A) Cells plated on circular FN-coated micropatterns and stained for paxillin (green), F-actin (red) and nuclei (DAPI, blue). Scale bar: 10 µm. The lower panel shows examples of the quantification of stress fibre length (red lines) and junctions (white crosses). (B) Quantification of the percentage of cells with organized stress fibres to total cells, mean of stress fibre length per cell and number of junctions per cell. The two images show examples of organized and disorganized stress fibres. Graphs show the quantification of 5–20 cells per condition. **P*<0.05; ***P*<0.01; ****P*<0.001; *****P*<0.0001 (unpaired two-tailed *t*-test between WT pKO cells and Lfc KO pKO cells). Quantitative results are mean±s.e.m. for the percentage of organized stress fibres and stress fibre length and mean±s.d. for number of junctions/cell. (C) RhoA activity of indicated cells determined by G-Lisa. Graph shows quantification of three independent experiments. **P*<0.05; ns, not significant (ordinary one-way ANOVA between pKO-αv and other conditions, and pKO-β1 and pKO-β1 Lfc KO). Results are mean±s.e.m. (D) Lfc activity of indicated cells determined by western blotting after GST–RhoA-G17A pulldown. Graph shows quantification of five independent experiments. ***P*<0.01 (one-sample *t*-test to theoretical mean 1 between pKO-αv and pKO-β1, pKO-αv and pKO-αv,β1). Quantitative results are mean±s.d.

These results confirmed that WT fibroblasts cultured on FN (bound by α5β1 and αv-class integrins) harboured EGFP–Lfc in the cytoplasm and on MTs, whereas antibody-mediated blockade of β1 integrins released EGFP–Lfc into the cytoplasm and αv-class integrin blockade with soluble cilengitide caused EGFP–Lfc to become associated with the MT network (Fig. S3A). Moreover, WT fibroblasts seeded on the αv-class integrin ligand VN, or β1-null deficient fibroblasts seeded on FN, also displayed a diffuse cytoplasmic distribution of EGFP–Lfc (Fig. S3A). Levels of active Lfc were also decreased after treatment with cilengitide, whereas blocking α5β1 integrins was without effect (Fig. S3B,C). Altogether, these findings strongly indicate that αv-class integrin engagement triggers Lfc release from MTs.

The release of Lfc from MTs can occur in cells by depolymerizing MTs, dissociating Lfc from the MT-associated Tctex-1–DIC complex after LPA or thrombin stimulation and/or direct phosphorylation of Lfc (Krendel et al., 2002; Meiri et al., 2012; Meiri et al., 2014; Fujishiro et al., 2008; von Thun et al., 2013; Patel and Karginov, 2014; Sandí et al., 2017; Yoshimura and Miki, 2011). Given that we performed our experiments under serum-free conditions, we can exclude a major involvement of LPA- and thrombin-mediated GPCR signalling in the αv-class integrin-induced Lfc release from MTs. MT dynamics of the three cell lines were similar after nocodazole washout, MT fractionation, and stability assays were performed (Fig. S4), indicating that the marked Lfc release from MTs in pKO-αv is not caused by unstable or depolymerized MTs. Therefore, release of Lfc from MTs in pKO-αv could be associated with differential phosphorylation of Lfc in these cells.

Lfc is differentially phosphorylated in pKO-αv and pKO-β1 fibroblasts

To investigate whether Lfc is differentially phosphorylated in pKO-αv, pKO-β1 and pKO-αv,β1 fibroblasts, we performed an unbiased phospho-enrichment proteomic analysis. We found that phospho-peptides carrying the five serine residues (S129, S151, S174, S931 and S959; see asterisks in Fig. S5A) in Lfc were significantly more enriched in pKO-αv than in pKO-β1 fibroblasts.

To determine whether these phospho-sites are involved in the release of Lfc from MTs, we replaced all five serine residues with alanine and expressed the resulting GFP-tagged Lfc-S5A in FN-seeded pKO-αv fibroblasts carrying a Crispr/Cas9-mediated deletion of the *Arhgef2* gene. Remarkably, replacements of the five phospho-sites shifted the localization of the mutant Lfc from the cytoplasm to MTs (Fig. 4A,B). To further define the phospho-serine residue(s) promoting Lfc release from MTs in pKO-αv fibroblasts, we generated and transiently expressed Lfc mutants carrying individual serine replacements (GFP–Lfc S129A, GFP–Lfc-S151A, GFP–Lfc-S174A, GFP–Lfc-S931A and GFP–Lfc-S959A) in pKO-αv Lfc KO fibroblasts seeded on FN. GFP–Lfc-S151A was sequestered on MTs and GFP–Lfc-S174A showed a slight colocalization with MTs, whereas the remaining mutants were predominantly located in the cytoplasm (Fig. 4A,B), indicating that Lfc-S151 represents a major site for which phosphorylation triggers the dissociation of Lfc from MTs upon αv-class integrin engagement.

To test whether αv-class integrin-mediated phosphorylation of Lfc-S151 triggers the Lfc release from MTs and Lfc activation, we stably expressed WT GFP–Lfc, GFP–Lfc-S151A or GFP–Lfc-S151D in pKO-αv Lfc KO fibroblasts (Fig. S5B) and performed GST-tagged RhoA-G17A pulldown experiments. We found that binding of GFP–Lfc-S151A to RhoA-G17A was decreased, whereas binding increased when Lfc-S151 was substituted for the phospho-mimetic amino acid GFP-Lfc-S151D (Fig. 4C; Fig. S5C), indicating that Lfc-S151 phosphorylation affects localization and activity of Lfc.

Staurosporine affects Lfc localization and activity in pKO-αv fibroblasts

Given that Lfc localization is controlled by increased phosphorylation in pKO-αv fibroblasts, we treated these cells with the broad-range kinase inhibitor staurosporine or the broad-range phosphatase inhibitors sodium fluoride (NaF) and sodium orthovanadate (Na_3VO_4). Staining of endogenous Lfc revealed that the treatment of pKO-αv fibroblasts with a low dose (1 and 2 nM) of staurosporine changed localization of Lfc from the cytoplasm to MTs (Fig. 5A; Movie 1). In line with the Lfc translocation to MTs, staurosporine treatment also decreased formation of stress fibres and Lfc activity (Fig. 5B,C). The treatment of pKO-αv fibroblasts with NaF, to inhibit serine/threonine phosphatases, or with Na_3VO_4, to inhibit tyrosine phosphatases, had no apparent effect on Lfc distribution (Fig. S6A), suggesting that kinases rather than phosphatases are the main players in signalling downstream of αv-class integrins.

The involvement of S151 in Lfc localization was further confirmed by stably overexpressing WT GFP–Lfc and the phospho-mimetic GFP–Lfc-S151D in pKO-αv Lfc KO fibroblasts. The experiments revealed that staurosporine treatment induced the translocation of WT GFP–Lfc from the cytoplasm to MTs. In contrast, phospho-mimicking GFP–Lfc-S151D remained cytoplasmic both before and after staurosporine treatment (Fig. 5D,E), underscoring the role of Lfc-S151 phosphorylation for MT translocation in pKO-αv cells. Treatment of pKO-αv with staurosporine decreased overall Lfc phosphorylation, including phosphorylation of S151 as observed by unbiased phospho-enrichment proteomic analysis (Fig. S6B,C).

MARK2 and MARK3 kinases are involved in Lfc release from MTs

MARK2 and MARK3 are members of the evolutionarily conserved MT-affinity regulating kinases (PAR-1) serine/threonine kinase family shown to bind and phosphorylate Lfc/GEF-H1 at several serine residues. MARK2 has been reported to phosphorylate Lfc-S143, -S885 and -S959, and MARK3 Lfc-S151 (Yamahashi et al., 2011; Yoshimura and Miki, 2011; Sandí et al., 2017). Nevertheless,

Journal of Cell Science (2023) 136, jcs260740. doi:10.1242/jcs.260740

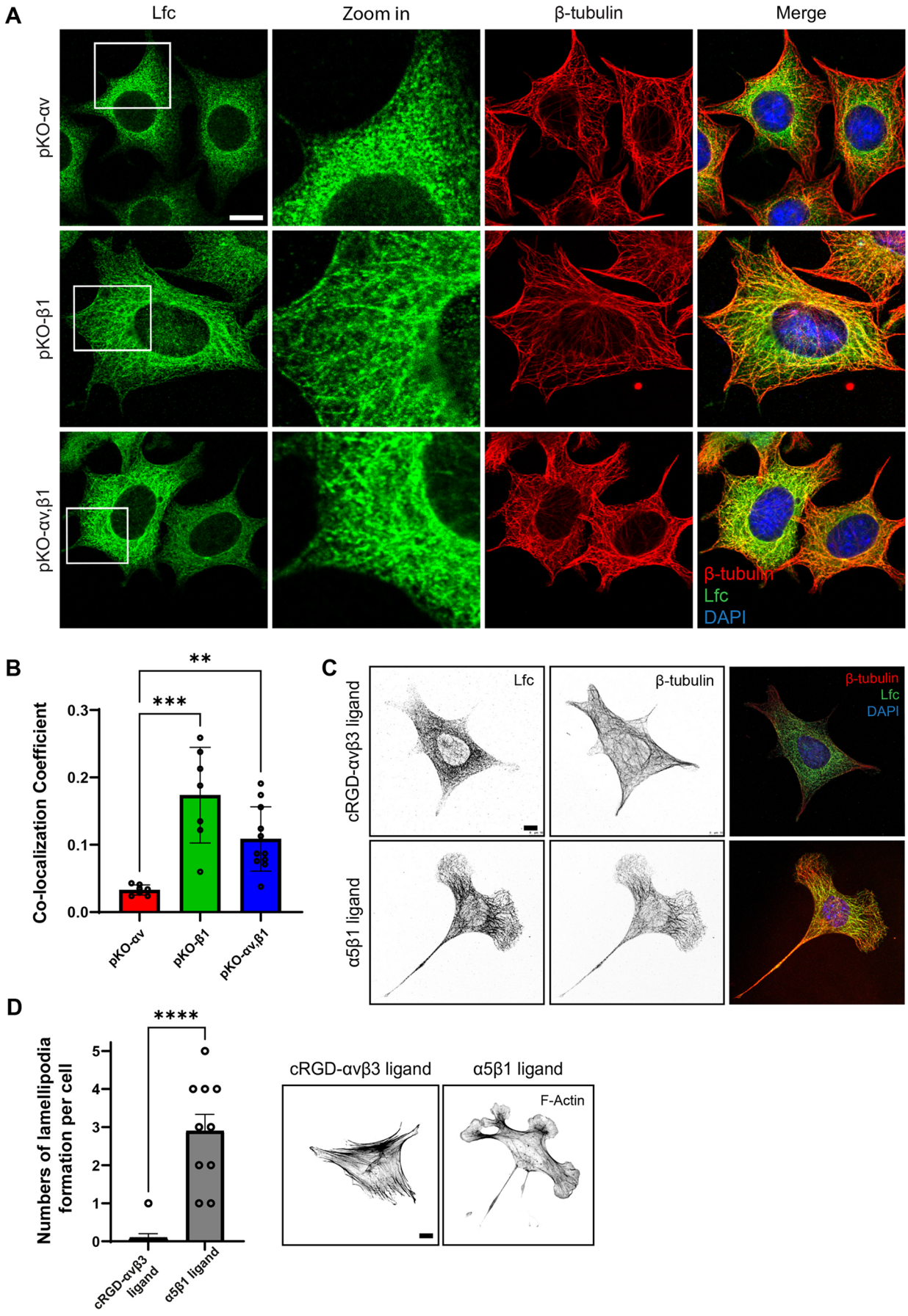

Fig. 3. See next page for legend.

Journal of Cell Science

Journal of Cell Science (2023) 136, jcs260740. doi:10.1242/jcs.260740

Fig. 3. Integrin-mediated control of subcellular Lfc localization. (A) The indicated cells were plated for 45 min on FN in serum-free medium and stained for Lfc (green), β-tubulin (red) and nuclei (DAPI, blue). Scale bar: 10 µm. (B) Quantification of colocalization between Lfc and β-tubulin. Graph show the quantification of 7–11 cells per condition from two independent experiments. ***P*<0.01; ****P*<0.001 (Kruskal–Wallis test between pKO-αv, pKO-β1 and pKO-αv,β1). (C) Immunostaining of WT mouse fibroblasts cultured for 60 min on glass coverslips coated with either c-RGD-αvβ3- or α5β1 specific peptidomimeticum in serum-free medium and then stained for Lfc (green), β-tubulin (red) and nuclei (DAPI, blue). Scale bar: 10 µm. (D) Quantification of number of protrusions per cell. Graph shows the quantification of 10 cells per condition. *****P*<0.0001 (unpaired two-tailed *t*-test between cRGD-αvβ3 ligand and α5β1 ligand). Grey scale images show F-actin. Scale bar: 10 µm. Quantitative results are mean±s.d.

MARK2 and MARK3 show high similarity in the N-terminal kinase domain and phosphorylate substrates at LXRXXSXXXL and KXGS motifs (Sonntag et al., 2019; Shackelford and Shaw, 2009; Trinczek et al., 2004; Drewes et al., 1997). Based on these similarities, we depleted MARK2 and/or MARK3 by siRNA and disrupted *MARK2* and *MARK3* genes by Crispr/Cas9 in pKO-αv fibroblasts (Fig. S6D,E). We observed an increased association of Lfc with MTs in MARK2 and MARK3-depleted cells, with a slightly more pronounced effect when both MARK2 and MARK3 expression were lost (Fig. 6A,B; Fig. S6F). This suggests that MARK2 and MARK3 operate downstream of αv-class integrins in mouse fibroblasts to regulate Lfc association with MTs.

In summary, these results indicate that αv-class integrin engagement with FN activates a signalling cascade resulting in the activation of MARK2 and MARK3 kinases, which trigger phosphorylation of Lfc at S151, leading to the release from MTs, activation of RhoA, induction of stress fibres and FA maturation.

DISCUSSION

Little is known about how different integrins differentially control Rho GTPase activity through the regulation of GEFs and we therefore aimed to identify and characterize GEFs involved in integrin signalling. We demonstrate that FN-binding αv-class integrins stimulate activation and alter subcellular localization of the RhoA-specific GEF Lfc (GEF-H1 in humans). We found that αv-class, but not β1, integrins induce high phosphorylation of Lfc and its translocation from MTs to the cytoplasm, followed by Lfc and RhoA activation and stress fibre formation. This does not exclude the role of β1 integrin in activating RhoA in a normal cell setting. However, in our system, activation of RhoA by Lfc was more pronounced in cells expressing only αvβ3 compared to that in β1 integrin-expressing cells, and expression of α5β1 seemed to have a counter-balancing effect to the αvβ3 signalling on RhoA activation as evidenced by the pKO-αv,β1 phenotype. pKO-αv,β1 cells, which show similarity with the WT phenotype, had almost as much activation of Lfc as pKO-αv cells, but similar RhoA activation to that in pKO-β1 cells. This indicates that although αvβ3 stimulates the activation of Lfc, if α5β1 is present, levels of RhoA activation will remain at WT levels.

Lfc was first described as an oncogene in NIH 3T3 fibroblasts (Whitehead et al., 1995), exhibiting the particularly interesting feature of localizing to MTs, which serves as an important link for actin-microtubule crosstalk (Krendel et al., 2002; Azoitei et al., 2019). We suggest that neither MT depolymerization/unstable MTs (Krendel et al., 2002) nor Gα-mediated dissociation of Lfc from the MT-resident Tctex-1–DIC complex (Meiri et al., 2014) play significant roles in the Lfc release from MTs in pKO-αv cells. Instead, we identified phosphorylation as the major Lfc regulator in response to αv integrins.

Several kinases have been shown to phosphorylate Lfc at various serine and threonine residues (Meiri et al., 2012; Meiri et al., 2014; Fujishiro et al., 2008; Patel and Karginov, 2014; Sandí et al., 2017; Meiri et al., 2009; Yamahashi et al., 2011), often resulting in Lfc activation. Our unbiased phospho-enrichment proteomic analysis revealed that Lfc was highly phosphorylated in pKO-αv cells when compared to in pKO-β1 cells, supporting a model in which increased Lfc phosphorylation upon αv-class integrin engagement leads to increased Lfc and RhoA activity. Interestingly, not only do pKO-αv,β1 cells show high activation of the same phospho-sites as pKO-αv cells but also of S885 and S959 (Fig. S5A), which have been linked to Lfc inhibition (Yamahashi et al., 2011). This might hint to a balanced Lfc regulation in these cells, where both αvβ3 and α5β1 integrins are expressed, leading to an even higher activation of the phospho-sites observed for the pKO-αv cells to balance the activation of the inhibitory sites S885 and S959 by α5β1 integrins. Given that activation of Lfc and RhoA and formation of thick stress fibres connected to large FAs were less pronounced in pKO-αv,β1 cells compared to pKO-αv cells, this further supports our hypothesis that αvβ3 and α5β1 integrins counter balance each other in regulating Lfc and RhoA signalling in WT mouse fibroblasts.

We found that S151 has a critical role in the subcellular localization and activation of Lfc in pKO-αv cells. However, we cannot discard that other phospho-sites identified in our unbiased phospho-enrichment proteomic analysis could contribute to Lfc activity in pKO-αv cells, since regulation of Lfc is a highly complex and multi-step process (Joo and Olson, 2021). Furthermore, low dose treatment with the broad kinase inhibitor staurosporine was able to efficiently induce the translocation of Lfc from the cytoplasm to MTs in pKO-αv fibroblasts. In addition, staurosporine treatment decreased RhoA activity and reduced stress fibre formation in pKO-αv cells, which is similar to the phenotype observed in Lfc-depleted pKO-αv cells. Hence, this suggests that kinases are involved in FN-engaged αvβ3 integrin-mediated Lfc and RhoA activation, stress fibre formation and FA maturation.

The importance of MARK3-mediated Lfc phosphorylation on S151 and its release from MTs was previously described by Sandí et al. (2017). As expected, depletion of MARK3 in pKO-αv cells led to Lfc association with MTs. Interestingly, depletion of MARK2 also led to the same phenotype, suggesting that both kinases can regulate Lfc in our system. MARK2 has been shown to phosphorylate different phospho-sites, which mostly lead to Lfc activation and translocation to the cytoplasm (Yoshimura and Miki, 2011). Inhibition of the phosphorylation of these sites due to MARK2 depletion in combination with the inhibition of S151 by MARK3 depletion could lead to a more pronounced effect in comparison to depletion of MARK2 or MARK3 alone. The same was observed when five serine residues (S5A) were mutated in comparison to S151A alone (Fig. 4A). Pasapera et al. (2022) has shown that MARK2 can associate with FAs via its membrane-binding domain, which suggests that MARKs could be activated by integrins at the FAs. In addition, Zuidema et al. (2022) has shown that β5 integrin can be regulated by MARK2, which shows a link of this kinase to the integrin signalling. Indeed, our pKO-αv cells express αvβ5 integrins. However, given that our experiments were performed on FN, αvβ5 might not play a role in MARK2 signalling in our system. Therefore, the association of MARK2 signalling with αvβ3 integrin could happen at the integrin level by a still unknown mechanism or through an unidentified kinase that might operate downstream of αv-class integrins and upstream of MARK2 and

Journal of Cell Science (2023) 136, jcs260740. doi:10.1242/jcs.260740

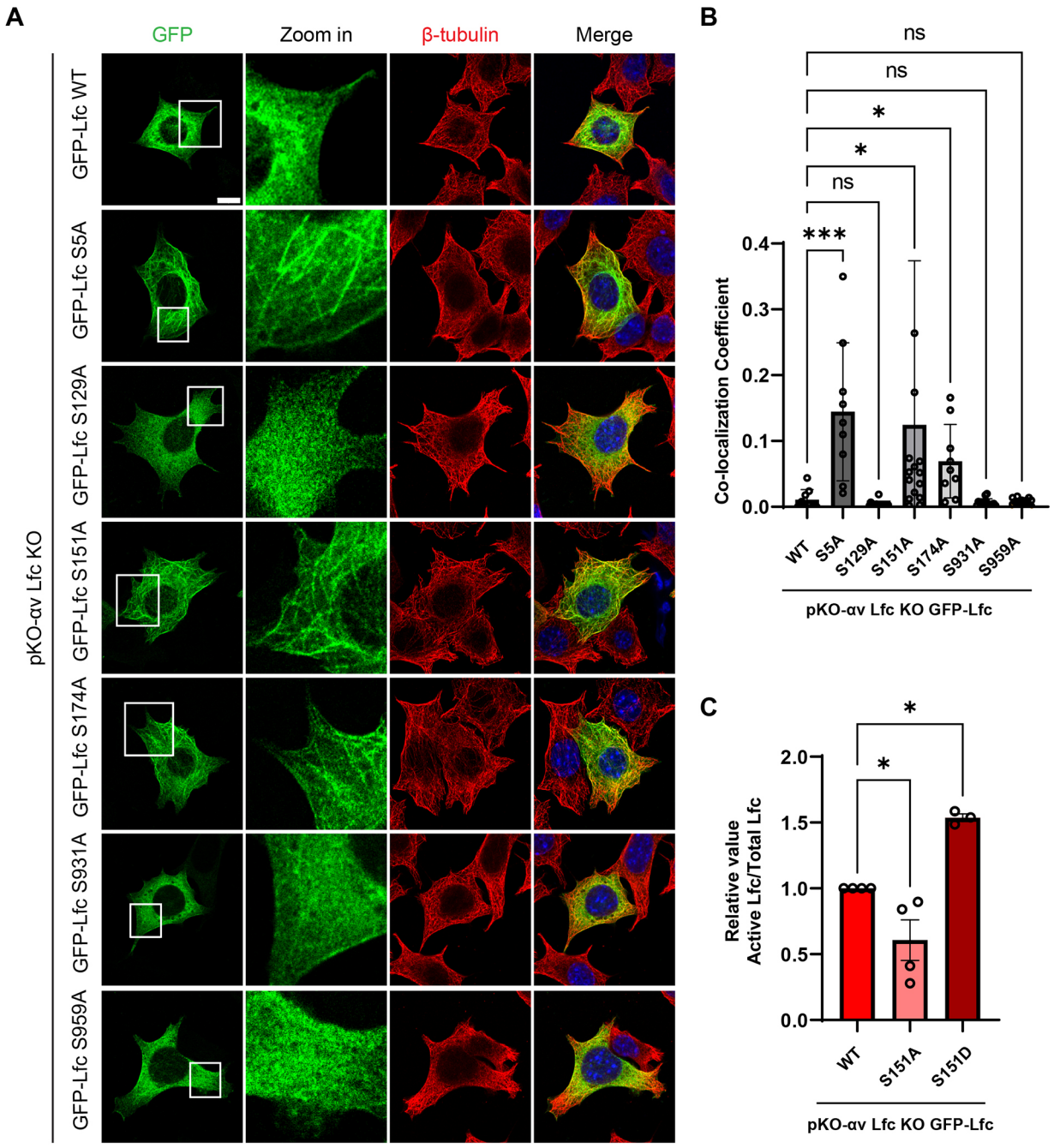

Fig. 4. Impact of Lfc phosphorylation on subcellular localization and activity. (A) pKO-αv Lfc KO cells overexpressing the indicated GFP–Lfc constructs cultured for 45 min on FN in serum-free medium and then visualized or stained for GFP–Lfc (green), β-tubulin (red) and nuclei (DAPI, blue). Scale bar: 10 µm. (B) Quantification of colocalization between GFP–Lfc and β-tubulin. Graph shows the quantification of 9–15 cells from three independent experiments. **P*<0.05; ****P*<0.001; ns, not significant (Kruskal–Wallis test between pKO-αv Lfc KO GPF WT and other mutants). Results are mean±s.d. (C) Lfc activity in pKO-αv Lfc KO cells stably expressing GFP–Lfc-WT, GFP–Lfc-S151A or GFP–Lfc-S151D determined by western blotting after GST–RhoA-G17A pull-down. Graph shows quantification of four independent experiments. **P*<0.05 (ordinary one-way ANOVA followed by Dunnett's test between GFP-Lfc-WT, GFP-Lfc-S151A and GFP-Lfc-S151D). Results are mean±s.e.m.

MARK3 in this pathway. A potential candidate is LKB1 (STK11), which has been shown to positively regulate MARKs (Lizcano et al., 2004; Timm et al., 2008) and to be involved in the translation of integrin signalling into cell polarity response (Chan et al., 2014).

Over the past decade, there has been a big emphasis on identifying key molecules and signalling pathways relevant to cellular mechanobiology. This study has shown that Lfc (GEF-H1) is an important link between specific integrin-ECM-sensing and RhoA activation, inducing changes in the cytoskeleton and cell contractility.

MATERIALS AND METHODS

Cell lines and reagents

Reconstituted pKO-αv, pKO-β1 and pKO-αv,β1 mouse fibroblast cell lines were generated as described by Schiller et al. (2013). Cells were grown in Dulbecco's modified Eagle's medium (DMEM) supplemented

Journal of Cell Science (2023) 136, jcs260740. doi:10.1242/jcs.260740

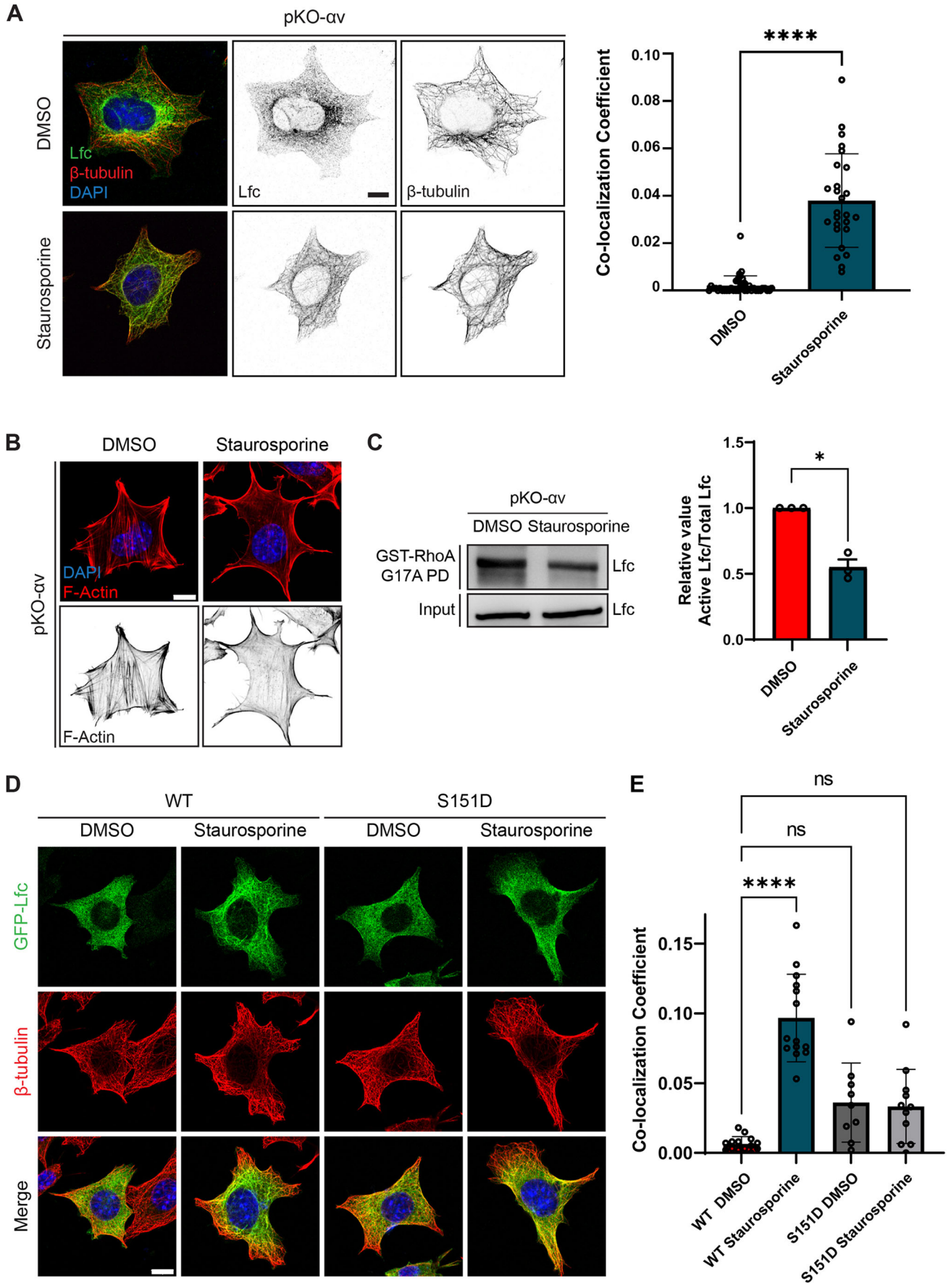

Fig. 5. See next page for legend.

Journal of Cell Science

Fig. 5. Staurosporine affects Lfc localization and activity in pKO-αv cells. (A) Immunostaining of pKO-αv cells plated on FN in serum-free medium and treated with staurosporine (2 nM). Graph shows the colocalization coefficient between Lfc and β-tubulin for 15 cells per condition. ****P<0.0001 (unpaired two-tailed t-test between DMSO and staurosporine). Scale bar: 10 µm. Quantitative results are mean±s.d. (B) pKO-αv cells plated on FN for 90 min in serum-free medium and treated with staurosporine, followed by F-actin (red) and nuclear staining (DAPI, blue). Images representative of three repeats. Scale bar: 10 µm. (C) Lfc activity was determined by western blotting after GST–RhoA-G17A pulldown of DMSO- and staurosporine-treated pKO-αv cells cultured for 4 h on FN in serum-free medium. Graph shows quantification of three independent experiments. *P<0.05; ns, not significant (one sample t-test to theoretical mean 1). Quantitative results are mean±s.e.m. (D) DMSO- and staurosporine-treated pKO-αv Lfc KO cells reconstituted with GFP–Lfc-WT or GFP–Lfc-S151D cultured for 90 min on FN in serum-free medium and then visualized or stained for GFP–Lfc (green), β-tubulin (red) and nuclei (DAPI, blue). Scale bar: 10 µm. (E) Quantification of colocalization between GFP–Lfc and β-tubulin. Graph shows the quantification of 10–14 cells from two independent experiments. ****P<0.0001; ns, not significant (Kruskal–Wallis test between pKO-αv Lfc KO GFP-WT DMSO and other conditions). Results are mean±s.d.

with 10% fetal bovine serum (FBS), 100 µg/ml streptomycin, and 100 U/ml penicillin (10270106 and 15140122, Gibco™; complete medium). The following antibodies and other reagents were used: anti-GEF-H1/Lfc [1:2000 (western blotting, WB) and 1:500 (immunofluorescence, IF), ab155785, Abcam], anti-β-tubulin (1:5000, T5201, Sigma, WB), anti-β-tubulin (1:50, E7-s, DSHB by Michael Klymkowsky, IF), anti-GAPDH (1:10,000, CB1001, Calbiochem®, Millipore, WB), anti-paxillin (1:300, 610051 clone 349, BD Transduction Laboratories, IF), anti-MARK2 (1:1000, #9118, Cell Signaling, WB), anti-MARK3 (1:1000, #9311, Cell Signaling), Rhodamine–phalloidin (1:300, R415, Molecular Probes, Invitrogen, IF), Alexa Fluor 488 anti-rabbit-IgG (1:500, A11008, Invitrogen), Alexa Fluor 488 anti-mouse-IgG (1:400, A11029, Invitrogen), Alexa Fluor 546 anti-mouse-IgG (1:400, A11003, Invitrogen), DAPI (1:1000, Sigma-Aldrich), nocodazole (M1404, Sigma-Aldrich), bovine plasma FN (34163, Sigma-Aldrich), staurosporine (S1421, Selleckchem), NaF (Sigma-Aldrich), Na_3VO_4 (Sigma-Aldrich), anti-mouse integrin α5β1 monoclonal antibody (MAB2575, clone BMC5, Merck), cilengitide (Hölzel), cRGD-αvβ3 and α5β1 selective peptidomimetic ligand (Rechenmacher et al., 2013).

Expression vectors and site-directed mutagenesis

Mouse full-length pCDNA3.1-EGFP-Lfc (transient expression) was kindly provided by Dr Michael Sixt (IST Austria, Klosterneuburg, Austria) and pRetroQ-AcGFP1-C1 (stable expression) was purchased from Clontech. Site-directed mutations were performed using the QuikChange site-directed mutagenesis kit (Agilent Technologies). Lfc was subcloned into pUC19 vector (Addgene #50005) for the mutation reactions and then subcloned again into pCDNA3.1-EGFP vector or pRetroQ-AcGFP1-C1. The nucleotide changes were verified by DNA sequencing (MWG-Eurofins). The correctness of the construct was verified by DNA sequencing (MWG-Eurofins). pGEX-GST-RhoA G17A was kindly provided by Rafael García-Mata (University of Toledo, Spain).

Generation of stable cell lines

pKO-αv Lfc KO were retrovirally transduced with mouse Lfc WT or Lfc mutant cDNA (pRetroQ-AcGFP1-C1-Lfc WT or pRetroQ-AcGFP1-C1-Lfc mutant). Cells were FACS sorted and GFP–Lfc levels were adjusted to endogenous Lfc expression.

DNA and siRNA transfection

Cells were transfected with different plasmids using 1:2 ratio of Lipofectamine® 2000 (Invitrogen) in medium without serum and antibiotics. Medium was changed to complete medium 6 h after transfection. After 48 h of transfection, cells were lysed or fixed for immunostaining.

Cells were transfected with different siRNAs using Viromer® Blue (0.5 µl to every 25 nM siRNA, Lipocalix), following the manufacturer's instructions. siRNAs were from Dharmacon: D-001810-10-05 (control, non-targeting SMART pool), L-040137-00-0005 (mouse MARK2 SMART pool), L040138-00-0005 (mouse MARK3 SMART pool), L-047092-00-0005 (mouse Arhgef1 SMART pool), L-040120-00-0005 (mouse Arhgef2 SMART pool), L-055988-01-0005 (mouse Arhgef5 SMART pool), L-049560-00-0005 (mouse Arhgef11 SMART pool), L-160106-00-0005 (mouse Akap13 SMART pool), L-045026-01-0005 (mouse Ect2 SMART pool) and L-051060-01-0005 (mouse Plekhg5 SMART pool). After 48 h of transfection, cells were lysed or fixed for immunostaining.

Active GEF pulldown assays

The protocol was performed as described by García-Mata et al. (2006) and Guilluy et al. (2011). Briefly, cells were seeded on FN 2 days before experiments. Cells were serum-starved for at least 3 h, detached with trypsin-EDTA and kept in suspension in serum-free medium for 1 h. Cells were re-seeded on FN in serum-free medium for the desired time points at 37°C, 5% CO_2. Lysis was performed on ice using lysis buffer (20 mM HEPES pH 7.5, 150 mM NaCl, 5 mM $MgCl_2$, 1% Triton X-100, protease inhibitor and phosphatase inhibitor). After clarification, lysates were incubated with GST–RhoA-G17A coupled to glutathione beads for 45 min at 4°C in an end-over-end mixer. A small aliquot was kept as loading control. Beads were washed with lysis buffer, resuspended in 2× Laemmli buffer and boiled for 5 min. Samples were either used for mass spectrometry analysis or western blotting.

G-Lisa RhoA activation assay

Cells were serum-starved overnight, detached with trypsin-EDTA and kept in suspension in serum-free medium for 1 h. Cells were then plated on FN-coated dishes (blocked with 1% BSA) in serum-free medium for 45 min. RhoA activity was measured by G-Lisa RhoA activation assay kit (Cytoskeleton, Inc.), following the manufacturer's instructions. Briefly, cells were lysed on ice with cell lysis buffer supplemented with protease inhibitor cocktail. Lysates were clarified by centrifugation at 10,000 ***g*** at 4°C for 1 min. The protein concentration of all samples was equalized after concentration was determined using Precision Red™ Advanced Protein Assay Reagent. Cell lysis buffer mixed with binding buffer was used as a blank and Rho control protein mixed with binding buffer was used as a positive control. Equalized lysates were mixed with binding buffer and added to the wells containing Rho GTP binding protein as well as the blank and positive control. After 30 min incubation under orbital shaking at 4°C, wells were washed twice with wash buffer and antigen presenting buffer was added to each well for 2 min at room temperature. Wells were washed again three times and anti-RhoA primary antibody was added to each well for 45 min at room temperature. After three washes, secondary antibody was added to each well for 45 min at room temperature. Signal was detected at absorbance 490 nm after HRP detection reagent incubation for 15 min at 37°C.

Western blotting

Lysates were resolved in SDS-polyacrylamide gels and transferred to PVDF membranes. Membranes were blocked in 5% (w/v) dried milk powder dissolved in Tris-buffered saline with 0.1% Tween 20 (TBS-T) and incubated with primary antibody overnight at 4°C. Membranes were washed three times with TBS-T and incubated for 1 h at room temperature with appropriated HRP-labelled secondary antibody. Enhanced chemiluminescence (Millipore) was used as a detection reagent. The original western blot images are shown in Figs S7 and S8.

Immunostaining

Cells were fixed with either 4% paraformaldehyde (PFA) for 15 min at room temperature or in methanol for 5 min at −20°C (anti-GEF-H1/Lfc and anti-β-tubulin). Cells were then permeabilized with 0.1% Triton X-100 in PBS for 5 min and blocked with 3% BSA with 0.1% Triton X-100 in PBS for 30 min. Cells were incubated with the required antibody in 1% BSA with 0.1% Triton X-100 in PBS overnight at 4°C followed by the incubation with the secondary antibody and phalloidin probe for 45 min. DAPI was used for nuclear staining. Confocal images were acquired with an inverted confocal microscope (Leica SP5 and Carl Zeiss LSM510).

Journal of Cell Science (2023) 136, jcs260740. doi:10.1242/jcs.260740

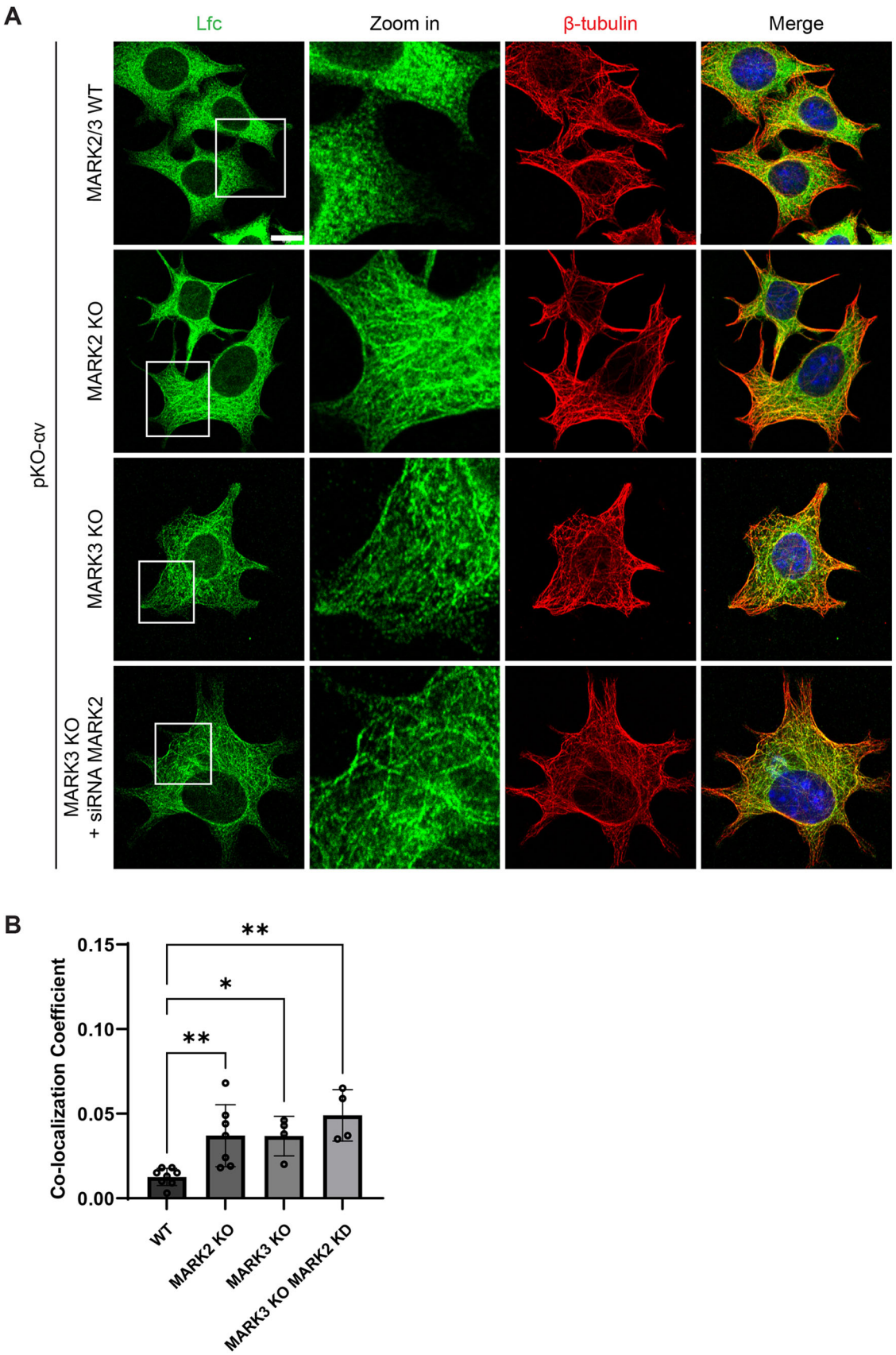

Fig. 6. MARK2 and MARK3 kinases mediate the Lfc release from MTs. (A) Indicated cells cultured for 45 min on FN in serum-free medium stained for Lfc (green), β-tubulin (red) and nuclei (DAPI, blue). Scale bar: 10 µm. (B) Quantification of colocalization between Lfc and β-tubulin. Graph shows the quantification of 4–8 cells from two independent experiments. *P<0.05 and **P<0.01 (Kruskal–Wallis test between pKO-αv Lfc KO GFP-WT DMSO and other conditions). Results are mean±s.d.

Journal of Cell Science (2023) 136, jcs260740. doi:10.1242/jcs.260740

Microtubule fractionation

MT fractionation was performed using a Microtubules/Tubulin In Vivo assay kit (Cytoskeleton), following the manufacturer's instructions. Briefly, cells were seeded on 10 cm FN-coated dishes 2 days before experiments. Cells were serum-starved for at least 3 h, detached with trypsin-EDTA and kept in suspension in serum-free medium for 1 h. Cells were re-seeded on FN in serum-free medium for 45 min at 37°C, 5% CO_2. Cells were washed with 37°C PBS and an appropriate volume of 37°C lysis buffer was added to the plate. Cells were harvested and homogenized using a 200 µl pipet tip. Cells were centrifuged at 2000 ***g*** for 5 min at 37°C. Supernatants were transferred to a new microcentrifuge tube and the concentration of samples was normalized before the next step. A small aliquot was kept as a loading control. Samples were centrifuged at 100,000 ***g*** for 60 min at 37°C. After centrifugation, supernatants (soluble tubulin) were transferred to new microcentrifuge tubes and the pellets (MTs) were resuspended in MT depolymerization buffer. Samples were analysed by western blotting.

Microtubule cold stability

MT cold stability assays were carried out as described in Atkinson et al. (2018). Briefly, cells were seeded on a six-well plate coated with FN (blocked with 1% BSA). Cells were left to adhere for 90 min at 37°C, 5% CO_2. The plate was then placed on ice for 15 min to induce MT depolymerization. Cells were washed with PBS and 100 µl of PEM buffer [80 µM PIPES pH 6.8, 1 mM EGTA, 1 mM $MgCl_2$, 0.5% Triton X-100 and 25% (w/v) glycerol] was added for 3 min. The whole volume was collected into a new microcentrifuge tube and cells were briefly washed with additional 50 µl of PEM buffer. The volume was collected and 150 µl of PEM was mixed with 150 µl of 2× EB buffer (3% SDS, 60 mM sucrose, 65 mM Tris-HCl pH 6.8). This fraction contained the cold unstable MTs. The cells remaining on the plate were lysed using 300 µl of 1× EB buffer. This fraction contained the cold stable MTs. Laemmli buffer (5×) was added to the samples, and they were boiled for 5 min prior to analysis by western blotting.

Peptidomimeticum binding assay

Nanopatterned gold surfaces were generated as described in Rechenmacher et al. (2013). Briefly, glass coverslips were passivated with polyethylene glycol (PEG), to prevent nonspecific protein adsorption or cell binding to the substrate area surrounding or in between the gold nanoparticles. Gold nanoparticles presenting integrin αvβ3 (cRGD) or α5β1 peptidomimetics were fixed on glass coverslips.

Mouse fibroblasts were serum-starved for 3 h, detached with trypsin-EDTA and blocked with trypsin inhibitor. Cells were resuspended in DMEM containing 0.5% BSA and seeded (~2×10^3 cells) on nanopatterned gold surfaces. After 60 min, cells were fixed with methanol for 5 min at −20°C and permeabilized with 0.1% Triton X-100 in PBS for 5 min. Cells were blocked with 3% BSA in PBS for 30 min and then incubated with the required antibodies Confocal images were acquired with an inverted confocal microscope (Leica SP5).

Micropatterning

Micropatterns were generated as described by Schiller et al. (2013). For immunofluorescence microscopy, cells were serum-starved for 3 h, detached with trypsin-EDTA and kept in suspension in serum-free medium for 1 h. Cells were then seeded on FN-coated circular micropatterns in 0.5% FBS medium for 90 min. Cells were fixed with 3% PFA in PBS for 5 min at room temperature, washed with PBS, blocked with 1% BSA in PBS for 1 h at room temperature and then incubated with antibodies. The fluorescence images were collected with a laser scanning confocal microscope (Leica SP5).

Fibroblast attachment to FN and VN

WT fibroblasts were serum-starved for 3 h and transfected with 1 µg of DNA (GFP–Lfc or GFP control). After 24 h, cells were detached with trypsin-EDTA and treated with cilengitide or α5β1 blocking antibody for 1 h in suspension in serum-free medium. Cells were seeded for 45 min either on FN-coated (10 µg/ml) or VN-coated (2.5 µg/ml) glass coverslips. β1 null fibroblast were seeded on FN-coated glass coverslips as a control. Cells were fixed with 3% PFA in PBS for 5 min at room temperature, washed with PBS, blocked with 1% BSA in PBS for 1 h at room temperature and then incubated with antibodies. The fluorescent images were collected with a laser scanning confocal microscope (Leica SP5).

Treatment with inhibitors

Nocodazole (M1404, Sigma-Aldrich): cells were treated for 2 h with 0.5 µM nocodazole (dissolved in DMSO) diluted in serum-free medium. In control experiments, cells were treated with the same volume of DMSO. Images were acquired 15 min after washout.

Staurosporine (S1421, Selleckchem): cells were treated for 90 min (immunofluorescence) or 4 h (GST–RhoA-G17A pulldown) with 2 nM staurosporine (dissolved in DMSO) diluted in serum-free medium. For MS-phosphoenrichment and timelapse movie, cells were treated with 1 nM staurosporine. In control experiments, cells were treated with the same volume of DMSO.

Phosphatase inhibitor (Sigma-Aldrich): cells were treated with 0.1 mM Na_3VO_4 or 1 mM NaF for 30 min in serum-free medium.

Cilengitide (Hölzel): cells were treated for 1 h with 2 µM of cilengitide diluted in serum-free medium.

α5β1 integrin-blocking antibody (MAB2575, clone BMC5, Merck/Millipore): cells were treated for 1 h with 10 µg/ml of α5β1-blocking antibody diluted in serum-free medium.

C3 transferase-based Rho inhibitor treatment (Cytoskeleton, Denver, USA): cells were treated for 4 h with 2.0 µg/ml (dissolved in water) diluted in serum-free medium.

Mass spectrometry

Active GEF sample preparation

Samples from active GEF pulldown assays were separated by SDS-polyacrylamide gel electrophoresis on a 4–15% gradient gel. Gel was stained with Coomassie using the GelCode™ Blue Safe Protein Stain reagent (Thermo Fisher Scientific).

Gel lanes of interest were excised, chopped and washed twice with 150 µl of de-staining buffer (25 mM ammonium bicarbonate and 50% ethanol). Gel pieces were dehydrated twice in 150 µl of 100% ethanol and dried by vacuum centrifugation. Then, 50 µl of digestion buffer (25 mM Tris-HCl, 10% acetonitrile, 10 ng/µl of trypsin) was added. After incubation for 20 min on ice, 50 µl of ammonium bicarbonate buffer (25 mM) was added and the gel pieces were incubated at 37°C overnight.

Peptides in the supernatant were collected and additional peptides were extracted from the gel pieces by repeated incubation at 25°C in 100 µl of extraction buffer [3% trifluoroacetic acid (TFA), 30% acetonitrile], with a subsequent centrifugation and collection of the supernatants. Finally, the gel pieces were dehydrated by incubation at 25°C in 100 µl of 100% acetonitrile and the supernatant was unified with the supernatants from previous extraction steps. Acetonitrile was removed by vacuum centrifugation and 70 µl of 2 M Tris-HCl as well as 10 mM tris(2-carboxyethyl) phosphine and 40 mM 2-chloroacetamide was added. After incubation for 30 min at 37°C, peptides were acidified to 1% TFA and desalted using Stage Tips.

Phospho-proteome sample preparation

For phospho-proteome analysis, cells were serum-starved for 3 h, detached with trypsin-EDTA and kept in suspension in serum-free medium for 1 h. Cells were washed twice with PBS, detached using a cell scraper and pelleted by centrifugation. Cell pellets were lysed in 700 µl lysis buffer [8 M Urea, 30 mM 2-Cloroacetamide (Sigma-Aldrich), 5 mM Tris (2-carboxyethyl) phosphine (TCEP; PierceTM, Thermo Fisher Scientific), 1% Benzonase, 1 mM MgCl2 in 100 mM Tris, pH 8.0] by incubation at 37°C for 10 min and subsequent sonication using a Sonoplus Ultrasonic homogenizer (Bandelin). Samples were incubated once more at 37°C for 10 min and sonicated in a Bioruptor Plus sonication system (Diogenode) for 10×30 s at high intensity. Before digestion, the samples were diluted 1:4 with MS grade water (VWR). Samples were digested for 2 h at 37°C with

Journal of Cell Science (2023) 136, jcs260740. doi:10.1242/jcs.260740

1 µg of LysC and overnight at 37°C with 3 µg trypsin (Promega). The solution of peptides was then acidified with Trifluoroacetic acid (Merck) to a final concentration of 1%, followed by desalting via Sep-Pak C18 1cc vacuum cartridges (Waters). The cartridge was washed twice with 1 ml of 100% acetonitrile (ACN) and twice with 1 ml of 0.1 M acetic acid prior to sample loading. Subsequently, the cartridge was washed twice with 1 ml of 0.1 M acetic acid. Elution was done with 0.5 ml of 80% (v/v) acetonitrile (ACN) and 0.1 M acetic acid in Milli-Q water. Samples were vacuum dried. Phosphorylated peptides were enriched with Fe(III)-NTA cartridges (Agilent Technologies; Santa Clara, Ca) using the AssayMAP Bravo Platform (Agilent Technologies; Santa Clara, Ca) in an automated fashion. Cartridges were primed at a flow rate of 100 µl/min with 250 µl of priming buffer (0.1% TFA, 99.9% ACN) and equilibrated at a flow-rate of 50 µl/min with 250 µl of loading buffer (0.1% TFA, 80% ACN). The flow-through was collected into a separate plate. Dried samples were dissolved in 200 µl of loading buffer and loaded at a flow-rate of 5 µl/min onto the cartridge. Cartridges were washed with 250 µl of loading buffer at a flow-rate of 20 µl/min and cross-linked peptides were eluted with 35 µl of 10% ammonia directly into 35 µl of 10% formic acid. Samples were dried down and stored at −20°C prior to further use. Before to LC–MS/MS analysis, the samples were resuspended in 10% formic acid.

LC-MS/MS data acquisition

Purified and desalted peptides were loaded onto a 30 cm column (inner diameter: 75 microns; packed in-house with ReproSil-Pur C18-AQ 1.9-micron beads, Dr. Maisch GmbH) via the autosampler of the Thermo Easy-nLC 1000 (Thermo Fisher Scientific) at 60°C. Using the nanoelectrospray interface, eluting peptides were directly sprayed onto the benchtop Orbitrap mass spectrometer Q Exactive HF (Thermo Fisher Scientific). Peptides were loaded in buffer A (0.1% formic acid) at 250 nl/min and percentage of buffer B (80% acetonitrile, 0.1% formic acid) increased from 2% to 30% over 120 min, followed by an increase to 60% over 10 min and then 95% over the next 5 min. Percentage of buffer B was maintained at 95% for another 5 min. The mass spectrometer was operated in a data-dependent mode with survey scans from 300 to 1650 m/z (resolution of 60,000 at m/z =200), and up to 10 of the top precursors were selected and fragmented using higher energy collisional dissociation (HCD with a normalised collision energy of value of 28). The MS2 spectra were recorded at a resolution of 15,000 (at m/z=200). AGC target for MS and MS2 scans were set to 3E6 and 1E5, respectively. For active GEFs, data acquisition was set within a maximum injection time of 100 and 60 min for MS and MS2 scans, respectively. Dynamic exclusion was set to 30 ms. For the phospho-proteome, data acquisition was used a maximum injection time of 20 ms for MS1 and 50 ms for MS2 scans. Dynamic exclusion was set to 16 ms.

Data analysis

Raw data were processed using the MaxQuant computational platform (version 1.6.5.0; Cox and Mann, 2008) with standard settings applied. Shortly, the peak list was searched against the Uniprot database of *Mus musculus* (55.466 entries) with an allowed precursor mass deviation of 4.5 ppm and an allowed fragment mass deviation of 20 ppm. MaxQuant, by default, enables individual peptide mass tolerances, which was used in the search. Cysteine carbamidomethylation, methionine oxidation and N-terminal acetylation, deamidation and phosphorylation were set as variable modifications. Proteins were quantified across samples using the label-free quantification algorithm in MaxQuant as label-free quantification (LFQ) intensities.

Bioinformatic analysis and heatmaps generation were made with the free access program Perseus, developed at Max Planck Biochemistry institute by Dr Jürgen Cox (https://maxquant.net/perseus/; Tyanova et al., 2016). The data corresponding to the biological replicates were filtered, based on valid values. Multiple testing corrections were performed. The mass spectrometry proteomics data have been deposited to the ProteomeXchange Consortium via the PRIDE partner repository (http://www.ebi.ac.uk/pride/archive/) with the dataset identifier PXD037596 (Active GEFs) and PXD037633 (Lfc phospho-proteome).

Crispr/Cas9 gene editing

For Lfc, guide RNAs were designed using the online tool (http://crispr.mit.edu/). Two Crispr gRNAs were selected, targeting the first translated exons (exons 2, common in all the splicing forms) of *Arhgef2* gene (Guide #1: score 85: 5′-GAGGTGGCCGTTGGTATAGC-3′; Guide #2: score 83: 5′-GCACATGGTCATGCCGGAGA-3′). A BbsI cut site was added and inserted into pX459 plasmid (Feng Zhang Lab - Addgene #62988). pKO-cells were transfected with 1 µg of pX459-gRNA1 or gRNA2, and pX459 alone as a control. Cells were treated for 3 days with puromycin (4 µg/ml), different clones were isolated and further characterized by western blotting, and the null mutation was confirmed by DNA sequencing of the targeted region using specific primers (MWG-Eurofins).

For MARK2 and MARK3, guide RNAs were designed following instructions on GeneArt™ Precision gRNA Synthesis Kit (Invitrogen). Two target sequences were selected for each gene (*MARK2*, 5′-CCCTACCCACGCTGAACGAA-3′ and 5′-GCTGACGAGCAGCCCCA-TAT-3′; *MARK3*, 5′-GAACTTTGCAAAAGTGAAAT-3′ and 5′-TACA-GACTGTTGAAAACAAT-3′). Sequences were checked using Blast (https://blast.ncbi.nlm.nih.gov/Blast.cgi). GeneArt™ Precision gRNA Synthesis Kit (Invitrogen) was used to synthase gRNA targeting mouse *MARK2* and mouse *MARK3* genes, following the manufacturer's instructions. Cells were transfected with gRNA and GFP-Cas9 (Invitrogen) using Viromer® Crispr (Lipocalix). Single cells were FACs sorted by GFP expression and grown in a 96-well plate. Clones were tested by western blotting and knockout was confirmed by DNA sequencing using specific primers for the targeted region (MWG-Eurofins).

Colocalization quantification

The colocalization of Lfc and β-tubulin was quantified using the colocalization tool in Zeiss Zen software version 2.3. The colocalization fraction was determined individually for each cell and individual thresholds were set accordingly. The colocalization coefficients were plotted as bar graphs and the appropriate statistical analysis was applied.

Stress fibre quantification

Stress fibre fluorescence intensity was quantified using ImageJ. The same threshold adjustments were used for all the images, followed by cell selection and measurement of the total fluorescent intensity.

The number of cells with ventral stress fibres was manually counted. Relative percentage of cells to total number of cells was calculated and plotted as bar graphs.

Organized and disorganized stress fibres, stress fibre length and junction number per cell were determined using the Ridge detection plugin from ImageJ. The parameters used for detection and fibres/junction quantification were line width 20.0, high contrast 230, low contrast 100, sigma 5, low threshold 0.0, and upper threshold 0.34.

FA quantification

Paxillin was used to mark FAs in pKO-cells adhered on FN-coated circular micropatterns. ImageJ was used to quantified FA sizes. The same threshold was applied for all the images and analysis was performed using the 'Analyze Particles' command. The parameters were set as size=0.06–10 and circularity=0.00–1.00. FA number was corrected on cell area.

Timelapse movies

Experiments were performed on pKO-αv cells attached on FN-coated glass without serum followed by treatment with 1 nM of staurosporine. Timelapse movie was acquired using a Leica SP8 confocal microscope.

Bioinformatics and statistics

Raw data were processed using the MaxQuant computational platform (Cox and Mann, 2008) with standard settings applied. Perseus was used to analyse the MS data and generate the heatmaps (Tyanova et al., 2016). Bar graphs and statistical analyses were generated in GraphPad Prism version 8.0.0 for Windows. The applied statistical methods are specified in the figure legends.

Acknowledgements
We thank Peter Krenn, Guan Wang, the Max Planck Institute of Biochemistry Imaging Facility and Max Planck Proteomic Facility for technical support, Reinhard Fässler for funding the project and editing the manuscript, and Anne Ridley for comments on the manuscript.

Competing interests
The authors declare no competing or financial interests.

Author contributions
Conceptualization: G.C., R.B.H.; Methodology: G.C., A.S., R.B.H.; Software: G.C., A.S., R.B.H.; Validation: G.C., R.B.H.; Formal analysis: G.C., A.S., R.B.H.; Investigation: G.C., A.S., R.B.H.; Data curation: G.C., R.B.H.; Writing - original draft: G.C., R.B.H.; Writing - review & editing: G.C., A.S., R.B.H.; Visualization: R.B.H., G.C.; Supervision: G.C., R.B.H.; Funding acquisition: G.C.

Funding
The work was funded by the Bundesministerium für Bildung und Forschung and Ministerio de Ciencia, Tecnología e Innovación Productiva (German-Argentinian Collaboration grant), Agencia Nacional de Promoción Científica y Tecnológica (PICT-Max Planck 2017-4685) and the Max Planck Society.

Data availability
The mass spectrometry proteomics data have been deposited to the ProteomeXchange Consortium via the PRIDE partner repository (http://www.ebi.ac.uk/pride/archive/) with the dataset identifier PXD037596 and PXD037633.

Peer review history
The peer review history is available online at https://journals.biologists.com/jcs/lookup/doi/10.1242/jcs.260740.reviewer-comments.pdf

References

Atkinson, S. J., Gontarczyk, A. M., Alghamdi, A. A., Ellison, T. S., Johnson, R. T., Fowler, W. J., Kirkup, B. M., Silva, B. C., Harry, B. E., Schneider, J. G. et al. (2018). The β3-integrin endothelial adhesome regulates microtubule-dependent cell migration. *EMBO Rep.* **19**, e44578. doi:10.15252/embr.201744578

Azoitei, M. L., Noh, J., Marston, D. J., Roudot, P., Marshall, C. B., Daugird, T. A., Lisanza, S. L., Sandí, M. J., Ikura, M., Sondek, J. et al. (2019). Spatiotemporal dynamics of GEF-H1 activation controlled by microtubule- and Src-mediated pathways. *J. Cell Biol.* **218**, 3077-3097. doi:10.1083/jcb.201812073

Barbieri, J. T., Riese, M. J. and Aktories, K. (2002). Bacterial toxins that modify the actin cytoskeleton. *Annu. Rev. Cell Dev. Biol.* **18**, 315-344. doi:10.1146/annurev.cellbio.18.012502.134748

Birkenfeld, J., Nalbant, P., Yoon, S. H. and Bokoch, G. M. (2008). Cellular functions of GEF-H1, a microtubule-regulated Rho-GEF: is altered GEF-H1 activity a crucial determinant of disease pathogenesis? *Trends Cell Biol.* **18**, 210-219. doi:10.1016/j.tcb.2008.02.006

Chan, K. T., Asokan, S. B., King, S. J., Bo, T., Dubose, E. S., Liu, W., Berginski, M. E., Simon, J. M., Davis, I. J., Gomez, S. M. et al. (2014). LKB1 loss in melanoma disrupts directional migration toward extracellular matrix cues. *J. Cell Biol.* **207**, 299-315. doi:10.1083/jcb.201404067

Chang, Y.-C., Nalbant, P., Birkenfeld, J., Chang, Z.-F. and Bokoch, G. M. (2008). GEF-H1 couples nocodazole-induced microtubule disassembly to cell contractility via RhoA. *Mol. Biol. Cell* **19**, 2147-2153. doi:10.1091/mbc.e07-12-1269

Costa, P., Scales, T. M., Ivaska, J. and Parsons, M. (2013). Integrin-specific control of focal adhesion kinase and RhoA regulates membrane protrusion and invasion. *PLoS One* **8**, e74659. doi:10.1371/journal.pone.0074659

Cox, J. and Mann, M. (2008). MaxQuant enables high peptide identification rates, individualized p.p.b.-range mass accuracies and proteome-wide protein quantification. *Nat. Biotechnol.* **26**, 1367-1372. doi:10.1038/nbt.1511

Danen, E. H. J., Sonneveld, P., Brakebusch, C., FäSsler, R. and Sonnenberg, A. (2002). The fibronectin-binding integrins α5β1 and αvβ3 differentially modulate RhoA–GTP loading, organization of cell matrix adhesions, and fibronectin fibrillogenesis. *J. Cell Biol.* **159**, 1071-1086. doi:10.1083/jcb.200205014

Drewes, G., Ebneth, A., Preuss, U., Mandelkow, E.-M. and Mandelkow, E. (1997). MARK, a novel family of protein kinases that phosphorylate microtubule-associated proteins and trigger microtubule disruption. *Cell* **89**, 297-308. doi:10.1016/S0092-8674(00)80208-1

Fujishiro, S. H., Tanimura, S., Mure, S., Kashimoto, Y., Watanabe, K. and Kohno, M. (2008). ERK1/2 phosphorylate GEF-H1 to enhance its guanine nucleotide exchange activity toward RhoA. *Biochem. Biophys. Res. Commun.* **368**, 162-167. doi:10.1016/j.bbrc.2008.01.066

García-Mata, R., Wennerberg, K., Arthur, W. T., Noren, N. K., Ellerbroek, S. M. and Burridge, K. (2006). Analysis of activated GAPs and GEFs in cell lysates. *Methods Enzymol.* **406**, 425-437. doi:10.1016/S0076-6879(06)06031-9

Guilluy, C., Dubash, A. D. and García-Mata, R. (2011). Analysis of RhoA and Rho GEF activity in whole cells and the cell nucleus. *Nat. Protoc.* **6**, 2050-2060. doi:10.1038/nprot.2011.411

Haga, R. B. and Ridley, A. J. (2016). Rho GTPases: regulation and roles in cancer cell biology. *Small GTPases* **7**, 207-221. doi:10.1080/21541248.2016.1232583

Hermann, M. R., Jakobson, M., Colo, G. P., Rognoni, E., Jakobson, M., Kupatt, C., Posern, G. and Fässler, R. (2016). Integrins synergise to induce expression of the MRTF-A-SRF target gene ISG15 for promoting cancer cell invasion. *J. Cell Sci.* **129**, 1391-1403. doi:10.1242/jcs.177592

Hodge, R. G. and Ridley, A. J. (2016). Regulating Rho GTPases and their regulators. *Nat. Rev. Mol. Cell Biol.* **17**, 496-510. doi:10.1038/nrm.2016.67

Hynes, R. O. (2002). Integrins: bidirectional, allosteric signaling machines. *Cell* **110**, 673-687. doi:10.1016/S0092-8674(02)00971-6

Joo, E. and Olson, M. F. (2021). Regulation and functions of the RhoA regulatory guanine nucleotide exchange factor GEF-H1. *Small GTPases* **12**, 358-371. doi:10.1080/21541248.2020.1840889

Krendel, M., Zenke, F. T. and Bokoch, G. M. (2002). Nucleotide exchange factor GEF-H1 mediates cross-talk between microtubules and the actin cytoskeleton. *Nat. Cell Biol.* **4**, 294-301. doi:10.1038/ncb773

Kuo, J.-C., Han, X., Hsiao, C.-T., Yates, J. R., 3RD and Waterman, C. M. (2011). Analysis of the myosin-II-responsive focal adhesion proteome reveals a role for β-Pix in negative regulation of focal adhesion maturation. *Nat. Cell Biol.* **13**, 383-393. doi:10.1038/ncb2216

Lizcano, J. M., Göransson, O., Toth, R., Deak, M., Morrice, N. A., Boudeau, J., Hawley, S. A., Udd, L., Mäkelä, T. P., Hardie, D. G. et al. (2004). LKB1 is a master kinase that activates 13 kinases of the AMPK subfamily, including MARK/PAR-1. *EMBO J.* **23**, 833-843. doi:10.1038/sj.emboj.7600110

Marjoram, R. J., Lessey, E. C. and Burridge, K. (2014). Regulation of RhoA activity by adhesion molecules and mechanotransduction. *Curr. Mol. Med.* **14**, 199-208. doi:10.2174/1566524014666140128104541

Meiri, D., Greeve, M. A., Brunet, A., Finan, D., Wells, C. D., Larose, J. and Rottapel, R. (2009). Modulation of Rho guanine exchange factor Lfc activity by protein kinase A-mediated phosphorylation. *Mol. Cell. Biol.* **29**, 5963-5973. doi:10.1128/MCB.01268-08

Meiri, D., Marshall, C. B., Greeve, M. A., Kim, B., Balan, M., Suarez, F., Bakal, C., Wu, C., Larose, J., Fine, N. et al. (2012). Mechanistic insight into the microtubule and actin cytoskeleton coupling through dynein-dependent RhoGEF inhibition. *Mol. Cell* **45**, 642-655. doi:10.1016/j.molcel.2012.01.027

Meiri, D., Marshall, C. B., Mokady, D., Larose, J., Mullin, M., Gingras, A. C., Ikura, M. and Rottapel, R. (2014). Mechanistic insight into GPCR-mediated activation of the microtubule-associated RhoA exchange factor GEF-H1. *Nat. Commun.* **5**, 4857. doi:10.1038/ncomms5857

Miao, H., Li, S., Hu, Y.-L., Yuan, S., Zhao, Y., Chen, B. P. C., Puzon-Mclaughlin, W., Tarui, T., Shyy, J. Y.-J., Takada, Y. et al. (2002). Differential regulation of Rho GTPases by β1 and β3 integrins: the role of an extracellular domain of integrin in intracellular signaling. *J. Cell Sci.* **115**, 2199-2206. doi:10.1242/jcs.115.10.2199

Narumiya, S., Tanji, M. and Ishizaki, T. (2009). Rho signaling, ROCK and mDia1, in transformation, metastasis and invasion. *Cancer Metastasis Rev.* **28**, 65-76. doi:10.1007/s10555-008-9170-7

Pasapera, A. M., Heissler, S. M., Eto, M., Nishimura, Y., Fischer, R. S., Thiam, H. R. and Waterman, C. M. (2022). MARK2 regulates directed cell migration through modulation of myosin II contractility and focal adhesion organization. *Curr. Biol.* **32**, 2704-2718.e6. doi:10.1016/j.cub.2022.04.088

Patel, M. and Karginov, A. V. (2014). Phosphorylation-mediated regulation of GEFs for RhoA. *Cell Adh. Migr.* **8**, 11-18. doi:10.4161/cam.28058

Rechenmacher, F., Neubauer, S., Polleux, J., Mas-Moruno, C., De, Simone, M., Cavalcanti-Adam, E. A., Spatz, J. P., Fässler, R. and Kessler, H. (2013). Functionalizing αvβ3- or α5β1-selective integrin antagonists for surface coating: a method to discriminate integrin subtypes in vitro. *Angew. Chem. Int. Ed. Engl.* **52**, 1572-1575. doi:10.1002/anie.201206370

Ren, Y., Li, R., Zheng, Y. and Busch, H. (1998). Cloning and characterization of GEF-H1, a microtubule-associated guanine nucleotide exchange factor for Rac and Rho GTPases. *J. Biol. Chem.* **273**, 34954-34960. doi:10.1074/jbc.273.52.34954

Roca-Cusachs, P., Gauthier, N. C., Del Rio, A. and Sheetz, M. P. (2009). Clustering of α.5β.1 integrins determines adhesion strength whereas α.vβ.3 and talin enable mechanotransduction. *Proc. Natl. Acad. Sci. USA* **106**, 16245-16250. doi:10.1073/pnas.0902818106

Sandí, M. J., Marshall, C. B., Balan, M., Coyaud, É., Zhou, M., Monson, D. M., Ishiyama, N., Chandrakumar, A. A., La Rose, J., Couzens, A. L. et al. (2017). MARK3-mediated phosphorylation of ARHGEF2 couples microtubules to the actin cytoskeleton to establish cell polarity. *Sci. Signal.* **10**, eaan3286. doi:10.1126/scisignal.aan3286

Schiller, H. B. and Fässler, R. (2013). Mechanosensitivity and compositional dynamics of cell-matrix adhesions. *EMBO Rep.* **14**, 509-519. doi:10.1038/embor.2013.49

Schiller, H. B., Hermann, M. R., Polleux, J., Vignaud, T., Zanivan, S., Friedel, C. C., Sun, Z., Raducanu, A., Gottschalk, K. E., Thery, M. et al. (2013). beta1- and alphav-class integrins cooperate to regulate myosin II during rigidity sensing

of fibronectin-based microenvironments. *Nat. Cell Biol.* **15**, 625-636. doi:10.1038/ncb2747

Shackelford, D. B. and Shaw, R. J. (2009). The LKB1–AMPK pathway: metabolism and growth control in tumour suppression. *Nat. Rev. Cancer* **9**, 563-575. doi:10.1038/nrc2676

Sonntag, T., Moresco, J. J., Yates, J. R., III and Montminy, M. (2019). The KLDpT activation loop motif is critical for MARK kinase activity. *PLoS One* **14**, e0225727. doi:10.1371/journal.pone.0225727

Timm, T., Marx, A., Panneerselvam, S., Mandelkow, E. and Mandelkow, E.-M. (2008). Structure and regulation of MARK, a kinase involved in abnormal phosphorylation of Tau protein. *BMC Neurosci.* **9**, S9. doi:10.1186/1471-2202-9-S2-S9

Trinczek, B., Brajenovic, M., Ebneth, A. and Drewes, G. (2004). MARK4 is a novel microtubule-associated proteins/microtubule affinity-regulating kinase that binds to the cellular microtubule network and to centrosomes. *J. Biol. Chem.* **279**, 5915-5923. doi:10.1074/jbc.M304528200

Tyanova, S., Temu, T., Sinitcyn, P., Carlson, A., Hein, M. Y., Geiger, T., Mann, M. and Cox, J. (2016). The Perseus computational platform for comprehensive analysis of (prote)omics data. *Nat. Methods* **13**, 731-740. doi:10.1038/nmeth.3901

Vial, E., Sahai, E. and Marshall, C. J. (2003). ERK-MAPK signaling coordinately regulates activity of Rac1 and RhoA for tumor cell motility. *Cancer Cell* **4**, 67-79. doi:10.1016/S1535-6108(03)00162-4

Von Thun, A., Preisinger, C., Rath, O., Schwarz, J. P., Ward, C., Monsefi, N., Rodríguez, J., Garcia-Munoz, A., Birtwistle, M., Bienvenut, W. et al. (2013). Extracellular signal-regulated kinase regulates RhoA activation and tumor cell plasticity by inhibiting guanine exchange factor H1 activity. *Mol. Cell. Biol.* **33**, 4526-4537. doi:10.1128/MCB.00585-13

Whitehead, I., Kirk, H., Tognon, C., Trigo-Gonzalez, G. and Kay, R. (1995). Expression cloning of lfc, a novel oncogene with structural similarities to guanine nucleotide exchange factors and to the regulatory region of protein kinase C. *J. Biol. Chem.* **270**, 18388-18395. doi:10.1074/jbc.270.31.18388

Yamahashi, Y., Saito, Y., Murata-Kamiya, N. and Hatakeyama, M. (2011). Polarity-regulating kinase partitioning-defective 1b (PAR1b) phosphorylates guanine nucleotide exchange factor H1 (GEF-H1) to regulate RhoA-dependent actin cytoskeletal reorganization. *J. Biol. Chem.* **286**, 44576-44584. doi:10.1074/jbc.M111.267021

Yoshimura, Y. and Miki, H. (2011). Dynamic regulation of GEF-H1 localization at microtubules by Par1b/MARK2. *Biochem. Biophys. Res. Commun.* **408**, 322-328. doi:10.1016/j.bbrc.2011.04.032

Zuidema, A., Wang, W., Kreft, M., Bleijerveld, O. B., Hoekman, L., Aretz, J., Böttcher, R. T., Fässler, R. and Sonnenberg, A. (2022). Molecular determinants of αVβ5 localization in flat clathrin lattices - role of αVβ5 in cell adhesion and proliferation. *J. Cell Sci.* **135**, jcs259465. doi:10.1242/jcs.259465